Hindawi
Shock and Vibration
Volume 2018, Article ID 7828267, 14 pages
https://doi.org/10.1155/2018/7828267

Research Article

Infinite Element Static-Dynamic Unified Artificial Boundary

Zhiqiang Song, Fei Wang, Yujie Liu, and Chenhui Su

State Key Laboratory of Eco-hydraulics in Northwest Arid Region of China, Xi'an University of Technology, Xi'an, China

Correspondence should be addressed to Zhiqiang Song; szhiq2004@126.com

Received 23 January 2018; Accepted 21 May 2018; Published 5 July 2018

Academic Editor: Roberto Palma

Copyright © 2018 Zhiqiang Song et al. This is an open access article distributed under the Creative Commons Attribution License, which permits unrestricted use, distribution, and reproduction in any medium, provided the original work is properly cited.

The method, which obtains a static-dynamic comprehensive effect from superposing static and dynamic effects, is inapplicable to large deformation and nonlinear elastic problems under strong earthquake action. The static and dynamic effects must be analyzed in a unified way. These effects involve a static-dynamic boundary transformation problem or a static-dynamic boundary unified problem. The static-dynamic boundary conversion method is tedious. If the node restraint reaction force caused by a static boundary condition is not applied, then the model is not balanced at zero moment, and the calculation result is distorted. The static numerical solution error is large when the structure possesses tangential static force in a viscoelastic static-dynamic unified boundary. This paper proposed a new static-dynamic unified artificial boundary based on an infinite element in ABAQUS to solve static-dynamic synthesis effects conveniently and accurately. The static and dynamic mapping theories of infinite elements were introduced. The characteristic of the infinite element, which has zero displacement at faraway infinity, was discussed in theory. The equivalent nodal force calculation formula of infinite element unified boundary was deduced from an external wave input. A calculation and application program of equivalent nodal forces was developed using the Python language to complete external wave inputting. This new method does not require a static and dynamic boundary transformation and import of stress field and constraint counterforce of boundary nodes. The static calculation precision of the infinite element unified boundary is more improved than the viscoelastic static-dynamic unified boundary, especially when the static load is in the tangential direction. In addition, the foundation simulation range of finite field can be significantly reduced given the utilization of the infinite element static dynamic unified boundary. The preciseness of static calculation and dynamic calculation and static-dynamic comprehensive analysis are unaffected.

1. Introduction

The simulation of a semi-infinite far-field foundation in the static and dynamic interaction of a structure-foundation system is a controversial issue in the seismic field of engineering. For static problems, considering that the elastic restoration effect of a sufficient range foundation is necessary, an artificial boundary, such as fixed or roller boundary, is typically used. For dynamic problems, a dynamic artificial boundary was used at the surface of the sufficient range foundation to simulate elastic restoration and radiation damping effects given energy dissipation in an infinitive foundation. Considerable research has been conducted on all kinds of dynamic artificial boundaries. Such types of research are mainly concentrated on two major categories, that is, local and global artificial boundaries.

The commonly used local artificial boundaries include transmission [1, 2], viscous [3], and viscoelastic boundaries [4–6]. Viscoelastic boundary, compared with viscous boundary, added a spring-damping system, which not only can dissipate extroverted waves on the boundary but also simulates an elastic restoration effect of the faraway foundation. The viscoelastic boundary has high precision and improved stability [7–9].

Infinite element is a typical global artificial boundary. In 1973, Ungless first proposed the idea of the infinite element, which is used to solve the infinite domain simulation problem [10]. Several scholars have contributed to the improvement, dissemination, and application of infinity element [11–14]. Bettess proposed mapping an infinite element called Bettess element based on a mapping between the global and the local coordinates [13]. He then summarized the research results on infinite elements and published the first monograph called Infinite Elements in 1992 [15]. In recent years, certain researchers have applied infinite element to studying the dynamic interaction of structure foundation [16–20]. Yun

[21, 22] innovated the dynamic infinite element formula and studied the 2D- and 3D-layered soil-structure interaction problem in frequency and time domains. Numerous studies indicate that infinite element can easily harmonize with finite element and has remarkable advantages and practicability in simulation and approximate simulation infinite domain problems compared with boundary element and other numerical methods for solving infinite domain problems.

The effects of static and dynamic loads can be solved separately for general small deformation and linear elastic structures. The superposition of the two effects is the total effect of the structures. Superposition principle is inapplicable for large deformation and nonlinear elastic problems under strong earthquake action. Static and dynamic effects must be analyzed in a unified way. These effects involve the static-dynamic boundary transformation or static-dynamic boundary unified problem. Qi [23] improved the artificial boundary of the dynamic infinite element without considering the static-dynamic unified artificial boundary based on the infinite element. Gao described a static-dynamic boundary conversion method for large deformation and nonlinear structures [24]. First, the static effect is analyzed under static boundaries, such as fixed boundary. Second, the static boundary is replaced by the dynamic boundary, such as viscoelastic boundary. Static-stress field and boundary-node-constrained reaction obtained by static analysis are introduced. Simultaneously, the original static force loads are inputted to ensure that the structure remains in a balanced state at the dynamic calculation zero-time. Third, the dynamic load is applied to analyze a dynamic response. The static-dynamic total effect can be obtained. This method is tedious. If the node restraint reaction force caused by static boundary condition is not applied, then the model is not balanced at zero moment, and the calculation result is distorted.

Several researchers began to study the static-dynamic boundary unified problem to avoid the tedious work of the static-dynamic boundary conversion. Certain researchers apply the viscoelastic dynamic artificial boundary to the static problem directly. The viscoelastic dynamic boundary was proposed based on wave motion theory in an infinite homogeneous elastic medium. The numerical solution indicated a larger deviation than theory solution when the viscoelastic dynamic artificial boundary is used directly in a static analysis. Liu proposed a viscoelastic static-dynamic unified artificial boundary [25]. He modified the spring stiffness coefficients of the viscoelastic dynamic boundary to make the dynamic boundary suitable for static analysis. The unified boundary was used to solve the static-dynamic combination problem of a semi-infinite space body bearing normal static and point source vibration loads at the free surface. The results show that the unified boundary increases the accuracy of the static analysis. Moreover, the precision and stability of a dynamic analysis can still be ensured. However, the static numerical solution error for the tangential static force remains large. Gao studied the stress of the semi-infinite space body using the viscoelastic static-dynamic unified boundary [24]. He also observed a large deviation between the transverse stress obtained by numerical simulation and theoretical solution at the internal points in the soil. The deficiency of viscoelastic static-dynamic unified boundary will not affect the accuracy of the static analysis when the static effect is mainly caused by structural self-weight. However, the hydraulic structure, water pressure, and sand pressure flow only in a horizontal direction. This deficiency of the viscoelastic static-dynamic unified boundary makes viscoelastic static-dynamic unified boundary unsuitable for hydraulic structures.

This paper proposed a new static-dynamic unified artificial boundary based on an infinite element in ABAQUS to solve the static-dynamic synthesis effect conveniently and accurately. The characteristic of the infinite element, which has zero displacement at infinite faraway, was discussed. The equivalent nodal force calculation formula of infinite element unified boundary was deduced from the external wave input. The calculation and application program of the equivalent nodal forces was developed using the Python language to complete the external wave inputting. This new method does not require static and dynamic boundary transformation and import of stress field and constraint counterforce of boundary nodes. The static calculation precision of the infinite element unified boundary is more improved than the viscoelastic static-dynamic unified boundary, especially when the static load is in a tangential direction. In addition, the foundation simulation range of finite field can be significantly reduced given the use of infinite element static-dynamic unified boundary. The accuracies of static calculation, dynamic calculation, and static-dynamic comprehensive analysis are unaffected. The calculation efficiency is improved when infinite element static-dynamic unified boundary was used for large nonlinear analysis.

This paper is organized as follows. Section 2 introduces the static and dynamic mapping theory of infinite elements. The equivalent nodal force calculation formula of infinite element unified boundary was deduced from the external wave input. Section 3 verifies the accuracy of the infinite element unified boundary that is applied to static calculation, dynamic calculation, and static-dynamic comprehensive analysis by numerical examples of a semi-infinite body and a practical gravity dam. The results show that the new method is relatively simple and accurate. The new method is especially suitable for structures subjected to horizontal tangential static load action. The influence of foundation simulation range on the finite domain to static calculation and static-dynamic comprehensive analysis is also discussed when the infinite element static-dynamic unified boundary was used. Section 4 presents the conclusions.

2. Mapping Principle and Exogenous Wave Input Method of Infinite Element

2.1. Static Mapping of Infinite Element. The basic ideas of the static mapping of the infinite element are as follows. (1) Plane or space semi-infinite domain is mapped to a finite domain by applying the mapping function in geometry. (2) Elements in the finite domain are analyzed to calculate single stiffness matrix in accordance with finite element method. (3) Total

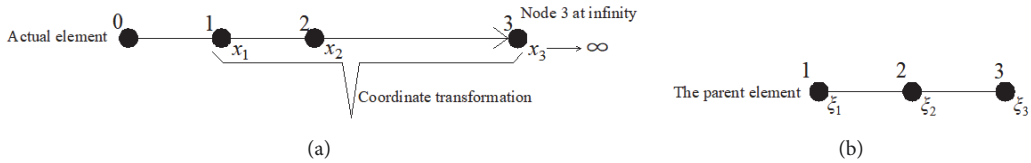

Figure 1: Static mapping of 1D infinite element.

stiffness matrix, stress, and displacement of the structure are obtained [19]. A type of 1D mapping infinite element is introduced.

Figure 1(a) illustrates an infinite element in the 1D X coordinate system. Nodes 1 and 2 are in the finite domain, whereas Node 3 is in the infinite domain. The infinite element in the X global coordinate system is transformed into the finite element (parent element) in ξ local coordinate system through the mapping function, as depicted in Figure 1(b). Then, we can use finite element theory in analyzing the parent element.

In Figure 1(a), the position coordinates of Nodes 1, 2, and 3 are assumed as x_1, x_2, and x_3, respectively. In Figure 1(b), the position coordinates of Nodes 1, 2, and 3 are ξ_1, ξ_2, and ξ_3, correspondingly. The node displacements are u_1, u_2, and u_3 in two coordinate systems.

The transformation relationship between the global and the local coordinates are as follows:

$$x = \sum_{i=1}^{2} M_i x_i, \tag{1}$$

where x_i are the node coordinates of the infinite element and M_i is the mapping function. $M_1 = -2\xi/(1-\xi)$ and $M_2 = (1+\xi)/(1-\xi)$. $x = x_1$ when $\boldsymbol{\xi_1} = -1$, and $x = x_2$ when $\boldsymbol{\xi_2} = 0$, where x tends to infinity when $\boldsymbol{\xi_3} = 1$ in the parent element. The infinitely far domain is mapped to a finite domain by constructing the mapping function and coordinate transformation between global and local coordinates.

The displacement mode of the element is as follows:

$$u = \sum_{i=1}^{3} N_i u_i, \tag{2}$$

where u_i denotes the node displacements and N_i stands for the shape functions $N_1 = 0.5\xi(\xi-1)$, $N_2 = (1-\xi^2)$, and $N_3 = 0.5\xi(1+\xi)$. The functions can be obtained by constructing the Lagrange polynomial $u=u_3=0$ when $\xi = 1$. The boundary condition that the displacement at infinity should be zero is satisfied.

The properties of the mapping infinite element are not introduced given the page limit. Additional information about this topic can be obtained from [16–19].

The infinite element simulates the infinite domain by mapping theory. The boundary condition that displacement is zero at infinity is satisfied in theory. For the structure-foundation system static interaction problem, using the infinite element to simulate the foundation at a distance from the structure is a high approximation method in actual engineering. However, the usual finite element model only intercepts the foundation near the structure according to Saint-Venant's Principle. The influence of the foundation that is distant from the structure is ignored. This method requires an interception range that is sufficiently large, thereby leading to an increase in the cost.

Figure 2: Semi-infinite elastic rod subjected to displacement disturbance.

2.2. Dynamic Mapping of the Infinite Element. For the wave problem of semi-infinite body, wave equation can be derived using elastic mechanics theory. The wave equation of an axial vibration half infinite long elastic rod could be deduced according to the relationship between stress and strain, relationship between displacement and strain, and dynamic equilibrium condition. In Figure 2, we assume that the rod was subjected to the displacement of $u_0=Ae^{iwt}$ disturbance at the end only. The wave equation is described in (3). The specific derivation process is discussed in [19].

$$\frac{\partial^2 u}{\partial x^2} = \frac{1}{C_P^2}\frac{\partial^2 u}{\partial t^2}, \tag{3}$$

where $C_P = \sqrt{E/\rho}$ is the propagating velocity of the longitudinal wave in the semi-infinite rod, E is the elastic modulus of the rod, ρ is the mass density of the rod, u is the displacement, A is the displacement amplitude, and ω is the excitation frequency.

In Figure 3, a 1D dynamic infinite element is assumed to be applied to the right end ($x=L$) of the semi-infinite elastic rod. It is equivalent to applying a mass damping and a spring boundary at the right end of the rod in elastic condition. Reference [19] sets the condition for not making the wave reflect at the boundary ($x=L$), as expressed in the following equation:

$$k - m\omega^2 = i\frac{\omega}{C_p}ES, \tag{4}$$

where k and m are the spring stiffness and quality of the rod right end, respectively. ω and C_p are the excitation frequency and wave velocity, correspondingly. E and S are the elastic modulus and cross-sectional area of the rod.

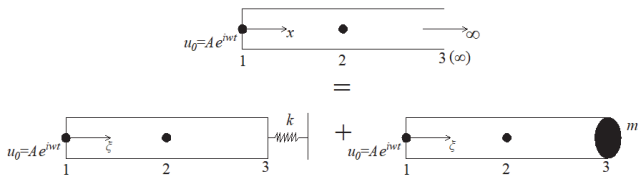

Figure 3: Dynamic mapping of a 1D infinite element.

The displacement mode of the wave in the semi-infinite elastic rod can be assumed as follows:

$$u = u_1 e^{-(\alpha+\beta i)\xi}, \tag{5}$$

where u_1 is the displacement of Node 1; $e^{-(\alpha+\beta i)\xi}$ is the propagation function of the wave; α is the displacement amplitude attenuation coefficient of the infinite element in a local coordinate system, which must be greater than zero; and β is the nominal wave number. Further discussions are available in [26].

The propagation function of the wave in infinite element local coordinate system is defined as

$$P(\xi) = e^{-(\alpha+\beta i)\xi}, \tag{6}$$

where α is a small number and $\beta = \omega/C_p$ is the nominal wave number. For viscoelastic materials, the values of α and β are related to the damping coefficient.

Then, the displacement mode of the infinite element can be defined as

$$u = u_1 N_1 = u_1 P(\xi), \tag{7}$$

where N_1 is the displacement shape function, as determined by the wave propagation characteristics, such as propagation direction, wave number, and amplitude attenuation coefficient. The 2D and 3D dynamic mapping infinite elements can be obtained in accordance with this principle.

The infinite element can be used to analyze the dynamic response of the structure-foundation system by coupling with the finite element. The condition that wave attenuation must be zero at the infinite faraway boundary can be satisfied automatically. The finite element model does not require applying other dynamic artificial boundaries, such as viscoelastic boundary, given the infinite element. The infinite element, as an artificial boundary, does not require a static and dynamic boundary transformation, import of stress field, and constraint counterforce of boundary nodes. In a combined static-dynamic analysis, the static node displacement is directly used as the initial displacement condition of the dynamic analysis.

2.3. Input of External Fluctuation of the Infinite Element. Lysmer and Kuhlemeyer's proposed infinite element dynamic artificial boundary theory is based on viscous boundary theory [3]. The difference is that the dampers are embedded uniformly in the infinite element. The free-field wave input mode of the infinite element boundary can check the viscous or viscoelastic artificial boundary theory. The free motion of seismic waves at the boundary can be converted to the equivalent nodal force that acts on the nodes in the coupling interface between infinite and finite elements. In recent years, the viscoelastic boundary has been improved and applied widely. The accuracy and stability are higher in the viscoelastic boundary than in the viscous boundary [7–9]. This research deduced ground motion input method of infinite element dynamic boundary based on viscoelastic boundary theory [4–7, 9].

The parallel spring-damper systems are connected to the artificial boundary node in the X, Y, and Z directions, while the other end is fixed.

The equivalent nodal force that acts on the artificial boundary node is expressed as follows: [9]

$$\boldsymbol{F}_b = \left(\boldsymbol{K}_b \boldsymbol{u}_b^{ff} + \boldsymbol{C}_b \dot{\boldsymbol{u}}_b^{ff} + \boldsymbol{\sigma}_b^{ff} \boldsymbol{n}\right) A_b, \tag{8}$$

where $\boldsymbol{u}_b^{ff}$ and $\dot{\boldsymbol{u}}_b^{ff}$ are the free-field displacement and velocity vectors at the artificial boundary, correspondingly; $\boldsymbol{u}_b^{ff} = [u\ v\ w]^T$, $\dot{\boldsymbol{u}}_b^{ff} = [\dot{u}\ \dot{v}\ \dot{w}]^T$, and $\boldsymbol{K}_\mathbf{b}$ and $\boldsymbol{C}_\mathbf{b}$ are the spring stiffness and damping coefficient of the physical component system, respectively; $\boldsymbol{\sigma}_\mathbf{b}^\mathbf{ff}$ is the free-field stress tensor, A_b is the affecting area of the artificial boundary node, and $\boldsymbol{n}$ are the cosine vectors of the outer normal direction of the artificial boundary. The first two items in (8) are used to balance the elastic recovery force and damping force produced by the spring and dampers on the artificial boundary node. The third term represents the nodal force generated by the free-field reaction.

The equivalent nodal force of the ground motion input could be obtained when $K_\mathrm{b} = 0$; this nodal force can be applied to the dynamic infinite element boundary. C_b has a specific expression form on different interfaces. When the outer normal line of the artificial boundary interface is in the X direction,

$$\boldsymbol{C_b} = \begin{bmatrix} C_{BN} & & \\ & C_{BT} & \\ & & C_{BT} \end{bmatrix} \text{ in the } Y \text{ direction,}$$

$$\boldsymbol{C_b} = \begin{bmatrix} C_{BT} & & \\ & C_{BN} & \\ & & C_{BT} \end{bmatrix} \text{ in the } Z \text{ direction,} \tag{9}$$

$$\text{and } \boldsymbol{C_b} = \begin{bmatrix} C_{BT} & & \\ & C_{BT} & \\ & & C_{BN} \end{bmatrix},$$

where C_BN and C_BT are the damping coefficients of dampers embedded in the dynamic infinite elements uniformly. $C_\mathrm{BN} = \rho C_\mathrm{P}$ and $C_\mathrm{BT} = \rho C_\mathrm{S}$. C_P and C_S are the wave velocities of P and S waves. The damping coefficient values are the same as the viscoelastic artificial boundary. Calculation and assignment of the coefficients are completed automatically through ABAQUS. Numerous preprocessing works have been avoided compared with the viscoelastic artificial boundary method.

We can assume that seismic wave has a vertical incidence at the bottom of the artificial boundary [27]. The equivalent

nodal forces of each node at different moments at each artificial boundary surface can be obtained by applying 1D wave theory. The specific expressions of equivalent nodal forces in a 3D model are defined as follows:

① Bottom surface:

$$\begin{aligned}
F_{bx}^{-z}(t) &= A_b\left(C_{BT}\left[\dot{u}_0(t)+\dot{u}_0\left(t-\frac{2H}{c_s}\right)\right]\right.\\
&\quad\left.+\rho c_s\left[\dot{u}_0(t)-\dot{u}_0\left(t-\frac{2H}{c_s}\right)\right]\right)\\
F_{by}^{-z}(t) &= A_b\left(C_{BT}\left[\dot{v}_0(t)+\dot{v}_0\left(t-\frac{2H}{c_s}\right)\right]\right.\\
&\quad\left.+\rho c_s\left[\dot{v}_0(t)-\dot{v}_0\left(t-\frac{2H}{c_s}\right)\right]\right)\\
F_{bz}^{-z}(t) &= A_b\left(C_{BN}\left[\dot{w}_0(t)+\dot{w}_0\left(t-\frac{2H}{c_p}\right)\right]\right.\\
&\quad\left.+\rho c_p\left[\dot{w}_0(t)-\dot{w}_0\left(t-\frac{2H}{c_p}\right)\right]\right),
\end{aligned} \tag{10}$$

where the superscript of the equivalent nodal force describes the outer normal line direction of the artificial boundary surface. The subscript of the equivalent nodal force describes the direction of the components. H is the distance from the boundary bottom surface to the ground. h is the node relative height of the bottom surface.

② Surface in X negative direction:

$$\begin{aligned}
F_{bx}^{-x}(t) &= A_b\left(C_{BN}\left[\dot{u}_0\left(t-\frac{h}{c_s}\right)+\dot{u}_0\left(t-\frac{2H-h}{c_s}\right)\right]\right.\\
&\quad\left.+\frac{\lambda}{c_p}\left[\dot{w}_0\left(t-\frac{h}{c_p}\right)-\dot{w}_0\left(t-\frac{2H-h}{c_p}\right)\right]\right)\\
F_{by}^{-x}(t) &= A_b\left(C_{BT}\left[\dot{v}_0\left(t-\frac{h}{c_s}\right)+\dot{v}_0\left(t-\frac{2H-h}{c_s}\right)\right]\right)\\
F_{bz}^{-x}(t) &= A_b\left(C_{BT}\left[\dot{w}_0\left(t-\frac{h}{c_p}\right)+\dot{w}_0\left(t-\frac{2H-h}{c_p}\right)\right]\right.\\
&\quad\left.+\rho c_s\left[\dot{u}_0\left(t-\frac{h}{c_s}\right)-\dot{u}_0\left(t-\frac{2H-h}{c_s}\right)\right]\right)
\end{aligned} \tag{11}$$

③ Surface in X positive direction:

$$\begin{aligned}
F_{bx}^{+x}(t) &= A_b\left(C_{BN}\left[\dot{u}_0\left(t-\frac{h}{c_s}\right)+\dot{u}_0\left(t-\frac{2H-h}{c_s}\right)\right]\right.\\
&\quad\left.-\frac{\lambda}{c_p}\left[\dot{w}_0\left(t-\frac{h}{c_p}\right)-\dot{w}_0\left(t-\frac{2H-h}{c_p}\right)\right]\right)\\
F_{by}^{+x}(t) &= A_b\left(C_{BT}\left[\dot{v}_0\left(t-\frac{h}{c_s}\right)+\dot{v}_0\left(t-\frac{2H-h}{c_s}\right)\right]\right)\\
F_{bz}^{+x}(t) &= A_b\left(C_{BT}\left[\dot{w}_0\left(t-\frac{h}{c_p}\right)+\dot{w}_0\left(t-\frac{2H-h}{c_p}\right)\right]\right.\\
&\quad\left.-\rho c_s\left[\dot{u}_0\left(t-\frac{h}{c_s}\right)-\dot{u}_0\left(t-\frac{2H-h}{c_s}\right)\right]\right)
\end{aligned} \tag{12}$$

④ Surface in Y negative direction:

$$\begin{aligned}
F_{bx}^{-y}(t) &= A_b\left(C_{BT}\left[\dot{u}_0\left(t-\frac{h}{c_s}\right)+\dot{u}_0\left(t-\frac{2H-h}{c_s}\right)\right]\right)\\
F_{by}^{-y}(t) &= A_b\left(C_{BN}\left[\dot{v}_0\left(t-\frac{h}{c_s}\right)+\dot{v}_0\left(t-\frac{2H-h}{c_s}\right)\right]\right.\\
&\quad\left.+\frac{\lambda}{c_p}\left[\dot{w}_0\left(t-\frac{h}{c_p}\right)-\dot{w}_0\left(t-\frac{2H-h}{c_p}\right)\right]\right)\\
F_{bz}^{-y}(t) &= A_b\left(C_{BT}\left[\dot{w}_0\left(t-\frac{h}{c_p}\right)+\dot{w}_0\left(t-\frac{2H-h}{c_p}\right)\right]\right.\\
&\quad\left.+\rho c_s\left[\dot{v}_0\left(t-\frac{h}{c_s}\right)-\dot{v}_0\left(t-\frac{2H-h}{c_s}\right)\right]\right)
\end{aligned} \tag{13}$$

⑤ Surface in Y positive direction:

$$\begin{aligned}
F_{bx}^{+y}(t) &= A_b\left(C_{BT}\left[\dot{u}_0\left(t-\frac{h}{c_s}\right)+\dot{u}_0\left(t-\frac{2H-h}{c_s}\right)\right]\right)\\
F_{by}^{+y}(t) &= A_b\left(C_{BN}\left[\dot{v}_0\left(t-\frac{h}{c_s}\right)+\dot{v}_0\left(t-\frac{2H-h}{c_s}\right)\right]\right.\\
&\quad\left.-\frac{\lambda}{c_p}\left[\dot{w}_0\left(t-\frac{h}{c_p}\right)-\dot{w}_0\left(t-\frac{2H-h}{c_p}\right)\right]\right)\\
F_{bz}^{+y}(t) &= A_b\left(C_{BT}\left[\dot{w}_0\left(t-\frac{h}{c_p}\right)+\dot{w}_0\left(t-\frac{2H-h}{c_p}\right)\right]\right.\\
&\quad\left.-\rho c_s\left[\dot{v}_0\left(t-\frac{h}{c_s}\right)-\dot{v}_0\left(t-\frac{2H-h}{c_s}\right)\right]\right)
\end{aligned} \tag{14}$$

3. Numerical Example Analyses

The following static, dynamic, and static-dynamic synthesis analyses not only involve the static and dynamic boundary but also include the static-dynamic unified boundary. To avoid confusion, a brief explanation on handling static, dynamic, and static-dynamic boundaries in each method was presented in Table 1.

Table 1: Illustration of boundaries in each method for different problems.

	Static problem	Dynamic problem	Static-dynamic synthetic problem
Method 1	Fixed boundary: Fully constrained at the bottom, normally constrained at side.	Viscoelastic dynamic artificial boundary.	Static-dynamic boundary transformation.
Method 2	Viscoelastic static-dynamic unified boundary: The stiffness coefficient of the spring has been corrected compared to the viscoelastic dynamic artificial boundary.	Viscoelastic static-dynamic unified boundary.	Viscoelastic static-dynamic unified artificial boundary.
Method 3	Infinite element static-dynamic unified boundary.	Infinite element static-dynamic unified boundary.	Infinite element static-dynamic unified boundary.

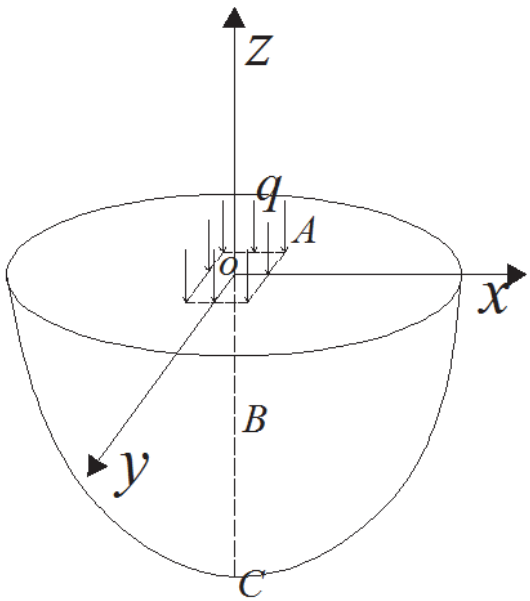

Figure 4: Semi-infinite body bearing normal uniform load.

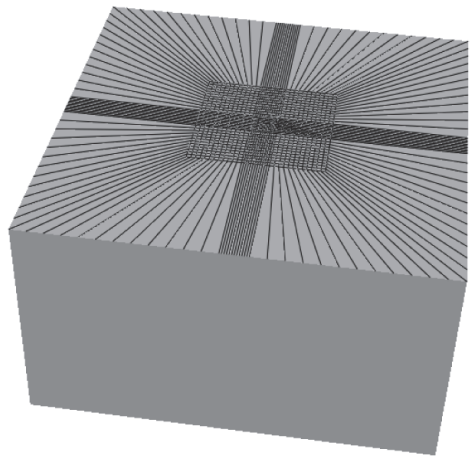

Figure 5: Finite-infinite element coupling model.

3.1. Semi-Infinite Body Bearing Normal Uniformly Distributed Static Load. In Figure 4, a rectangular uniformity distributed static load acted on the surface of a semi-infinite body vertically. The side length of the rectangle is 6.0 m. The mass density, elastic modulus, and Poisson ratio of the semi-infinite body are 1000 kg/m^3, 2.4×10^7 Pa, and 0.2, respectively. q is the rectangular uniformity distributed load defined by q=1×10^6 Pa. A discrete finite element model with the size of 60 m × 60 m × 50 m is intercepted in the semi-infinite domain. The coordinate origin is located at the center of the top surface of the model. Methods 1 and 2 were used on the finite element model to solve the static problem. Another finite-infinite coupling model was constructed (Figure 5). The finite elements are wrapped up by infinite elements. Method 3 was used on the finite-infinite coupling model to solve this static problem.

Points O, B, and C are the typical observation points with the coordinates (0,0,0), (0,0,−25), and (0,0,−50), respectively. The theoretical displacement solutions of these typical observation points in the Z direction could be deduced according to elastic mechanics [28]. The numerical displacement solutions in the Z direction obtained by using different boundary methods and their relative errors with the theoretical solution are summarized in Table 2.

Table 2 displays that the displacement precision of the infinite element static-dynamic unified artificial boundary is the highest among the three artificial boundary methods. In addition, we decreased the finite domain simulation range in Method 3 to 1/8 of the original size. We call it Method 4 to distinguish it from Method 3. Table 2 reflects that the decrease in finite domain simulation range did not significantly influence the accuracy of static displacement response in the Z direction of the semi-infinite body. Among Methods 1, 2, and 4, Method 4 is the most accurate. Method 4 improved computational efficiency while maintaining favorable accuracy in static analysis.

3.2. Semi-Infinite Body Bearing Tangential Concentrating Static Load on the Surface. A tangent concentrating force equal to 1×10^7 N acted as the semi-infinite body described

Table 2: Numerical displacements of different boundary methods and their relative errors.

Observation points	O		B		C	
	U_z (m)	Error (%)	U_z (m)	Error (%)	U_z (m)	Error (%)
Theory solution	−0.2693	0.00	−0.0292	0.00	−0.0147	0.00
Numerical solution of Method 1	−0.2737	1.63	−0.0176	−39.73	0.0000	Boundary effect
Numerical solution of Method 2	−0.2760	2.45	−0.0253	−13.36	−0.0106	−27.89
Numerical solution of Method 3	−0.2696	0.11	−0.0295	1.03	−0.0149	1.36
Numerical solution of Method 4	−0.2668	−0.92	−0.0318	8.90	−0.0134	−8.84

Table 3: Numerical displacements of different boundary methods and their relative errors.

Observation point	D		E		F		G	
	U_x(m)	Error (%)	U_x(m)	Error (%)	U_x(m)	Error (%)	U_x(m)	Error (%)
Theory resolution	0.0796	0.00	0.0398	0.00	0.0265	0.00	0.0199	0.00
Numerical solution of Method 1	0.7176	801	0.2550	540	0.1187	347	0.0393	97
Numerical solution of Method 2	0.7217	806	0.2592	551	0.1229	363	0.0436	119
Numerical solution of Method 3	0.6221	681	0.1562	292	0.0233	−12	0.0191	−4

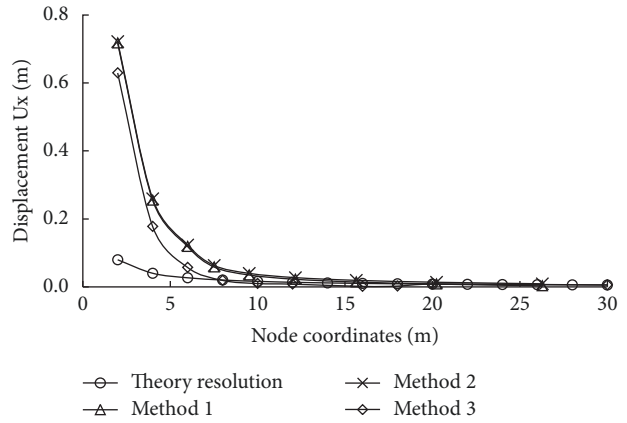

Figure 6: Theoretical and numerical displacements of different boundary methods.

in Section 3.1. Theoretical displacement solutions of typical observation points (D(2,0,0), E(4,0,0), F(6,0,0), and G(8,0,0)) on x-axis on the surface of the semi-infinite body can be deduced from the elastic mechanics [29]. The theoretical and numerical displacement solutions obtained using different boundary methods of these typical points are exhibited in Figure 6. The numerical displacement solutions and their relative error with the theoretical solutions are summarized in Table 3.

Figure 6 and Table 3 display that the displacement error is large near the tangential concentration force acting position. The calculation accuracy of the three artificial boundary methods increased gradually with the increase in the point X coordinate. The displacement error calculated by viscoelastic static-dynamic unified artificial boundary method could be easily found. This displacement error is the largest, and the precision is the worst among the three artificial boundary methods. The infinite element static-dynamic unified artificial boundary significantly improved the defective precision when tangential concentrating forces acted. The relative error of the observation point F obtained by the infinite element static-dynamic unified artificial boundary method is approximately 10%. Among these artificial boundaries, the infinite element static-dynamic unified artificial boundary has the lowest error and the highest accuracy.

3.3. Semi-Infinite Body Bearing Unit Impulse Dynamic Load. We also used the semi-infinite body described in Section 3.1 as an example. A unit impulse P wave in Z direction and a unit impulse S wave in X and Y directions were inputted to the semi-infinite body discrete model at the bottom. The unite impulse wave is expressed in (15). The wave velocities are C_P = 163.30 m/s and Cs = 100.00 m/s. The calculation time is 2.0 s.

$$u(t) = \frac{1}{2}\left[1 - \cos(8\pi t)\right] \quad 0 \le t \le 0.25$$
$$u(t) = 0 \quad 0.25 < t \le 2.0. \tag{15}$$

The theory displacements of points O, B, and C in Z direction obtained according to 2D wave theory are illustrated in Figure 7. The numerical displacements in Z direction of these observation points obtained by using three boundary methods are depicted in Figures 8–10. The maximum of the numerical displacements and their relative error compared with the theoretical solution are presented in Table 4.

The theory displacements of points D, E, and F in X direction can be obtained according to 1D wave theory. The numerical displacements in X direction of the three observation points could be obtained through the three boundary methods. The displacement history curves are similar to Figures 7–10. These displacement curves are no longer presented due to the page limit. The displacement

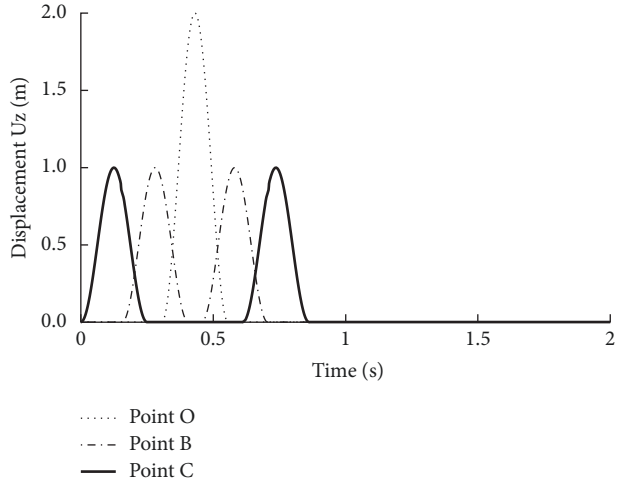

Figure 7: Theory displacement.

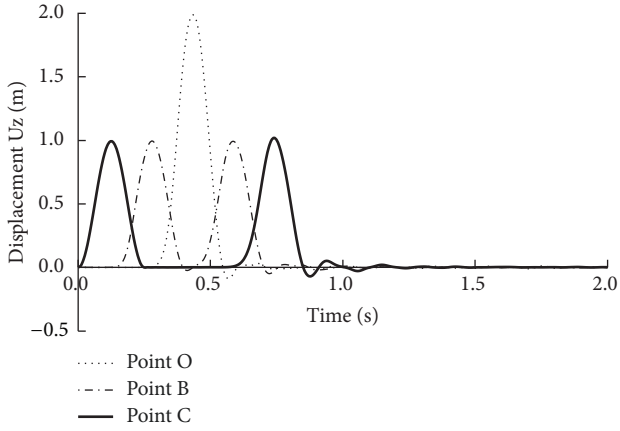

Figure 8: Numerical displacement of Method 1.

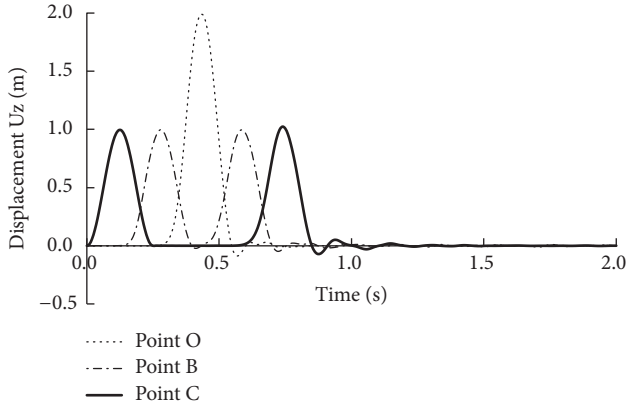

Figure 9: Numerical displacement of Method 2.

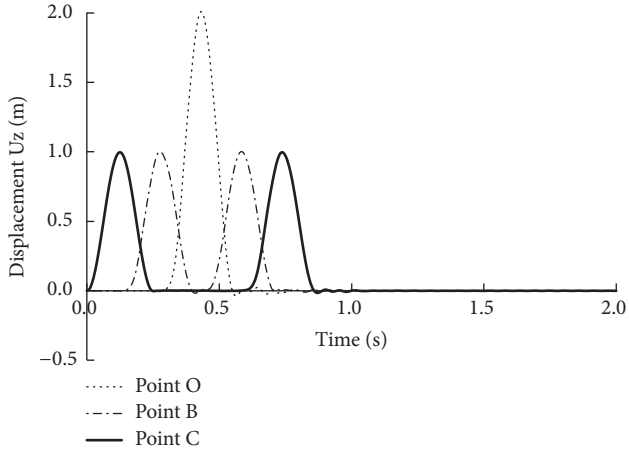

Figure 10: Numerical displacement of Method 3.

maximums of different boundary methods and their relative errors compared with theoretical solutions are presented in Table 5.

Figures 7–10 and Tables 4 and 5 display that the displacement waveforms of observation points obtained through the three artificial boundary methods are identical to the theoretical solution in either vertical or horizontal direction. The displacement maximums of the numerical solution at each point are close to the theoretical solution. The relative error is minimal. However, the waveforms obtained by using the viscoelastic dynamic boundary (Method 1) and the viscoelastic static-dynamic unified boundary (Method 2) have minimal amplitude oscillations when the outer traveling wave passes the boundary. The waveform obtained by using infinite element static-dynamic unified boundary (Method 3) has improved stability when the outer traveling wave passes the boundary.

3.4. Semi-Infinite Body Bearing Static-Dynamic Synthetical Load. The influence of different boundary methods to the static-dynamic synthesis effect of a semi-infinite body is studied in this section. First, the static uniformity load in the vertical direction and unit pulse dynamic load mentioned above acted on the semi-infinite body described in Section 3.1. Then, the tangential concentrating static force and unit pulse dynamic load mentioned above acted on the semi-infinite body.

The normal static uniformity load is acted on the surface of the model first, and then the zero dynamic load is inputted to the model to verify whether the model is balanced at the initial time in the dynamic calculation or not. The static-dynamic synthetical Z direction displacements history curves of points O and B obtained by different boundary methods are depicted in Figures 11 and 12. We can infer that the model that uses the infinite element static-dynamic unified boundary (Method 3) is in an equilibrium state at the termination time of static analysis (the initial time of dynamic analysis). The static-dynamic synthetical displacements maintained a constant value during the zero dynamic load acting process. Conversely, the model, which uses the static-dynamic boundary transformation method (Method 1), no longer maintains equilibrium at the initial time of dynamic analysis if the boundary nodal constraint reaction force is not imported. The static-dynamic synthetical displacements fluctuated during the zero dynamic load acting process. The infinite element static-dynamic unified

Table 4: Displacement maximums of different boundary methods and their relative errors in the Z direction.

Observation point	O		B		C	
	U_z (m)	Error (%)	U_z (m)	Error (%)	U_z (m)	Error (%)
Theory resolution	2.000	0.00	1.000	0.00	1.000	0.00
Numerical solution of Method 1	1.988	−0.6	0.995	−0.5	0.996	−0.4
Numerical solution of Method 2	1.988	−0.6	0.955	−0.5	0.955	−0.5
Numerical solution of Method 3	1.990	−0.5	0.993	−0.7	0.997	−0.3

Table 5: Displacement maximums of different boundary methods and their relative error in the X direction.

Observation point	D		E		F	
	U_x (m)	Error (%)	U_x (m)	Error (%)	U_x (m)	Error (%)
Theory resolution	2.000	0.00	2.000	0.00	2.000	0.00
Numerical solution of Method 1	1.983	−0.9	1.985	−0.8	1.990	−0.5
Numerical solution of Method 2	1.982	−0.8	1.984	−0.8	1.979	−1.1
Numerical solution of Method 3	2.014	0.7	2.009	0.5	2.007	0.4

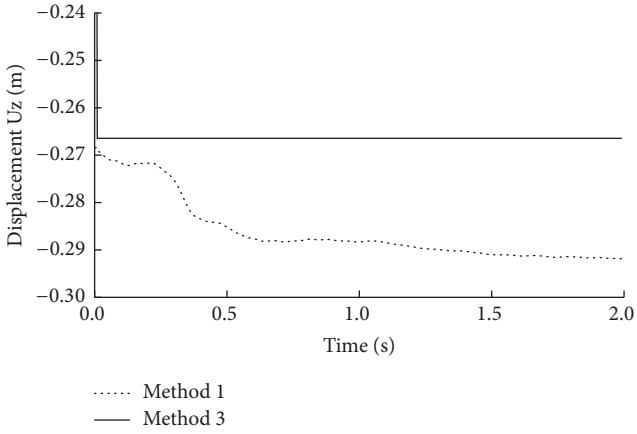

Figure 11: Displacements of Point O under zero dynamic load.

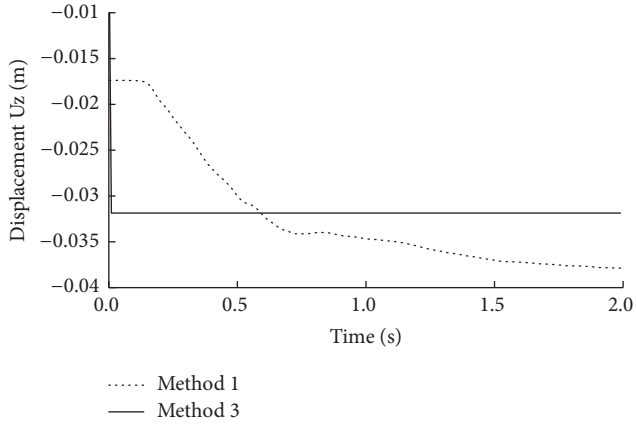

Figure 12: Displacements of Point B under zero dynamic load.

artificial boundary is feasible and suitable for static-dynamic synthetical analysis. The complicated process of importing the initial stress field and applying node constraint reaction force is avoided.

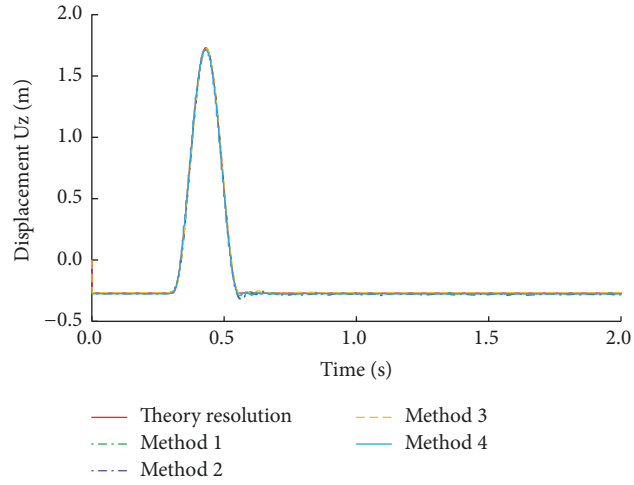

Figure 13: Z component displacement of Point O.

The numerical displacements of points O, B, and C in Z direction obtained by using three boundary methods are demonstrated in Figures 13–15. For convenience in the discussion of the performance of three kinds of boundaries, the theoretical solution obtained by superposition principle is also presented in Figures 13–15.

The theoretical and numerical displacement solutions of points D, E, and F in X direction obtained by using three boundaries are depicted in Figures 16–18 when the tangential concentrating static force and unit pulse dynamic load acted.

Figures 13–15 reflect that the deviation between the Z component displacements numerical solution calculated by three boundary methods and the theoretical solution is minimal when the normal static force and unit pulse dynamic load acted.

Figures 16–18 illustrate that the precision of the infinite element static-dynamic unified artificial boundary is better than the other two kinds of boundaries when the tangential concentrating static force and unit pulse dynamic load

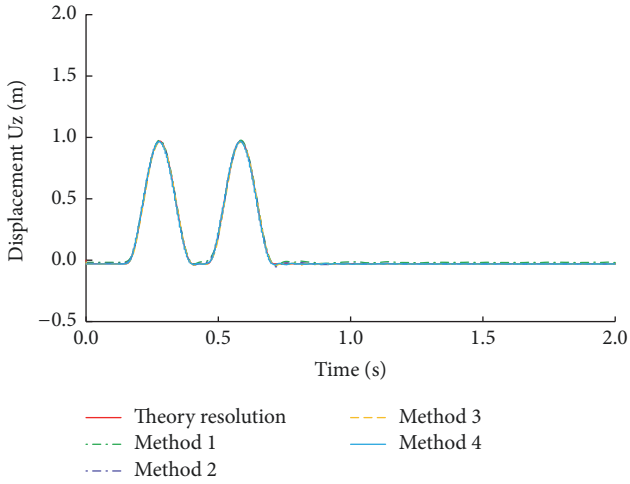

Figure 14: Z component displacement of Point B.

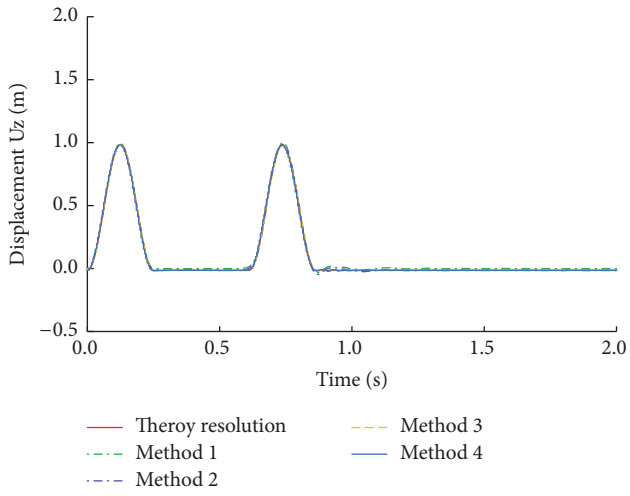

Figure 15: Z component displacement of Point C.

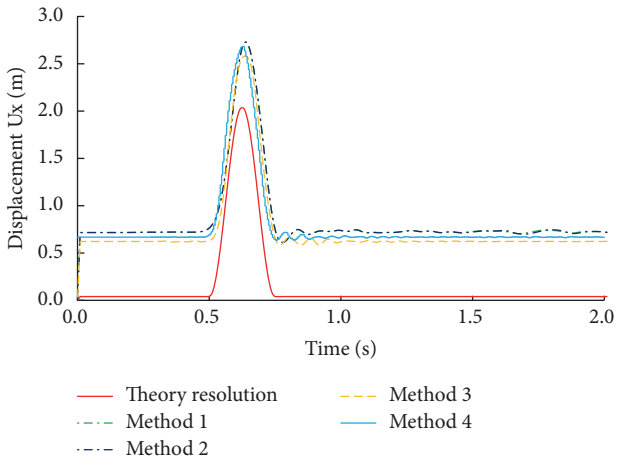

Figure 16: X component displacement of Point D.

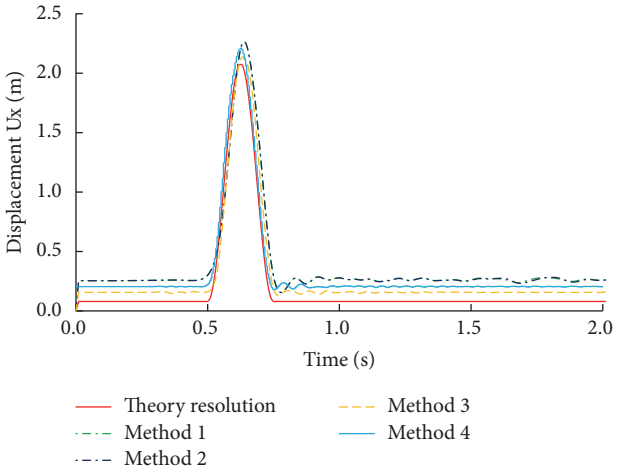

Figure 17: X component displacement of Point E.

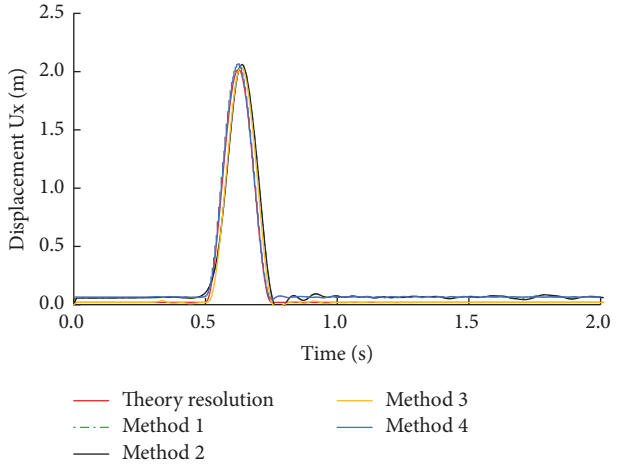

Figure 18: X component displacement of Point F.

acted. However, a certain error exists between the numerical solution obtained by infinite element static-dynamic unified boundary and theoretical solution when the point is near the tangential force action position. However, the infinite element static-dynamic unified artificial boundary is the most accurate among the other kinds of boundaries. The numerical solutions are near the theoretical solutions when the observation points are distant from the tangential concentration force action position.

In Tables 4 and 5, the precisions of the three boundaries are proximate when the model is subjected to impulse dynamic only. The error of the dynamic response has minimal contribution to the error of the comprehensive response. The error of the comprehensive response depends significantly on the error of the static effect. The infinite element static-dynamic unified boundary is suitable for static problem whether normal or tangential load acted or not. Therefore, the static-dynamic comprehensive response is closest to the theoretical solution among the boundaries.

In addition, we decreased the finite domain simulation range in Method 3 to 1/8 of the original size as presented in

Table 6: Analysis times of four different methods.

Methods	Vertical comprehensive response t/min	Tangential comprehensive response t/min
Method 1	103	81
Method 2	101	77
Method 3	46	38
Method 4	30	23

Section 3.1. We call it Method 4 In order to distinguish it from Method 3. Figures 13–18 demonstrate that the decrease in finite domain simulation range did not significantly influence the accuracy of static-dynamic comprehensive displacement response in Z or X direction of the semi-infinite body. Among Methods 1, 2, and 4, Method 4 remains the most accurate. Method 4 improved computational efficiency while maintaining favorable accuracy in the static-dynamic unified analysis. The infinite element static-dynamic unified boundary has excellent application prospect for large-scale nonlinear problem analysis.

Table 6 showed the analysis times of the four different methods under the same calculation conditions; the infinite element static-dynamic unified boundary can greatly save the calculation time.

3.5. Concrete Gravity Dam Bearing Static-Dynamic Synthetical Load. A 3D finite element model of a certain dam section of a concrete gravity dam was constructed. The height of the dam section is 100 m, while the width of the dam section is 66.5 m at the bottom and 7.0 m at the top. The upstream and downstream slope ratios are 0 and 0.7, respectively. The mass density, elastic modulus, and Poisson ratio of the dam body concrete are 2400 kg/m^3, 24.0 GPa, and 0.167, correspondingly. The mass density, elastic modulus, and Poisson ratio of the dam foundation rock are 2600 kg/m^3, 15.0 GPa, and 0.25, respectively. The intercept range of foundation rock is 100 m (one time of the dam height) in depth, upstream, downstream, left, and right directions. The normal upstream and downstream water levels are 95 and 9.7 m, correspondingly. The model coordinates origin is located at the center of the upstream side at the foundation surface. X, Y, and Z represent the direction of along flow, vertical flow, and vertical, respectively. The static loads include gravity, hydrostatic pressure, sediment pressure, and uplift pressure. The dynamic load is the seismic load. The dynamic water pressure is simulated by an additional mass at the corresponding position.

The static-dynamic comprehensive effect was calculated by using the three boundary methods mentioned above. The performance and applicability of the three boundaries are studied when they were used to solve hydrostructure static-dynamic analysis. The finite-infinite element coupling model is depicted in Figure 19. The infinite elements (element type: CIN3D8) are wrapped around the peripheral of the finite elements (element type: C3D8R).

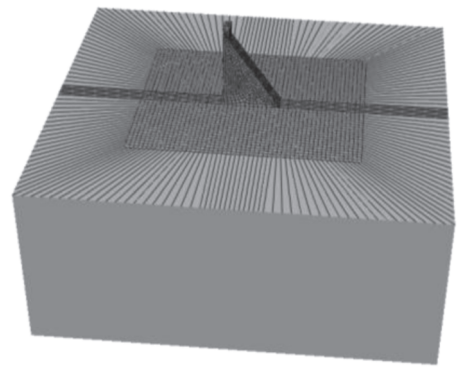

Figure 19: Finite-infinite element coupling model of the dam foundation system.

According to actual engineering site conditions and standard design response spectrum regulated by seismic design code for the structure of hydraulic engineering (NB 35047-2015) [30], the acceleration time history of ground motion is artificially fitted. The site type where the gravity dam is located is I_0, and the characteristic period of the site is 0.2 s. The maximum value of the standard design response spectrum is 2.0. The peak of ground horizontal motion acceleration is 0.1 g, while the peak acceleration of vertical ground motion is 0.067 g. The total calculation time is 20 s, and the time step is 0.01 s. The correlation coefficient between X and Y, Y and Z, and X and Z components is 0.043, 0.083, and −0.008, thereby satisfying the requirement of the standard (NB 35047-2015). The Rayleigh damping model with the damping constants of 0.0077 and 1.259 is adopted. The velocities and displacements time history can be obtained by numerical integration. Equivalent nodal forces can be calculated using the relative equations above, which were applied to the nodes at the boundaries of the finite domain.

The static-dynamic comprehensive relative displacements of upstream surface dam crest center in X and Z directions obtained by different boundary methods are demonstrated in Figures 20 and 21. The reference point is the origin of the coordinate. In Figures 20 and 21, the influence of the different boundaries to the relative displacements of the upstream surface dam crest center in X and Z directions is minimal. Figures 22 and 23 illustrate the maximums of the static-dynamic comprehensive relative displacements of upstream surface center at various height positions in X and Z directions. The maximums were normalized according to the maximums obtained through Method 3. The difference of

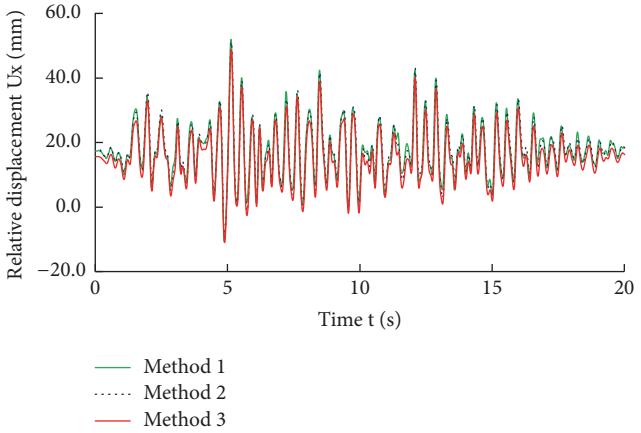

Figure 20: Time history curve of the X component relative displacement at the top of dam.

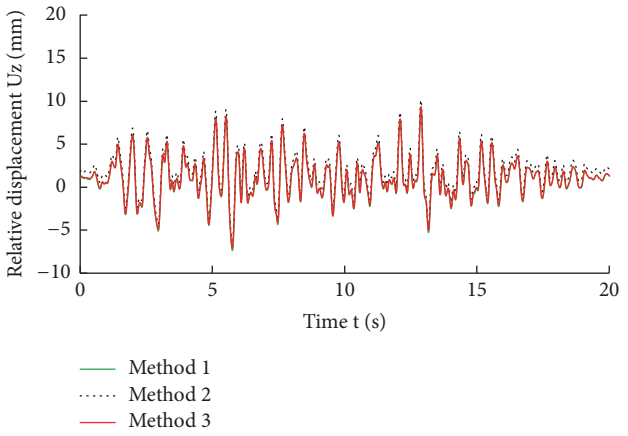

Figure 21: Time history curve of the Z component relative displacement at the top of dam.

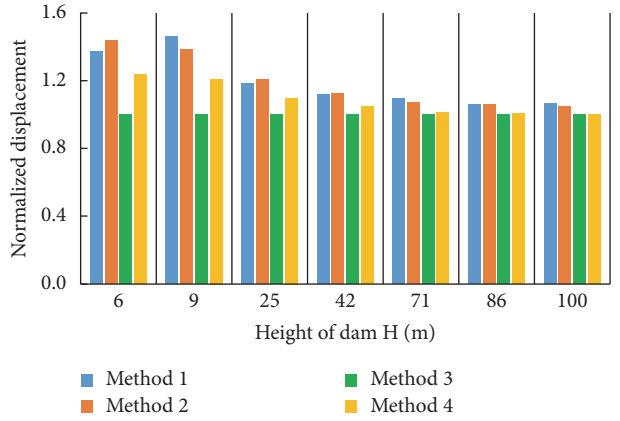

Figure 22: Normalized relative displacement in the x direction at different heights of the dam.

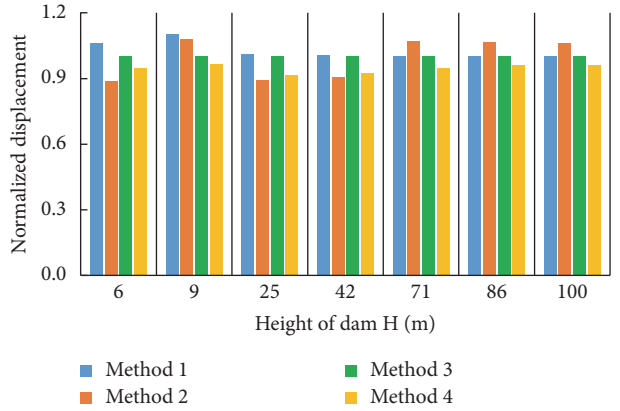

Figure 23: Normalized relative displacement in the z direction at different heights of the dam.

maximum relative displacements in Z direction obtained by using three boundaries along the dam height was maintained minimal. The accuracies of the three boundary conditions for the normal static and dynamic comprehensive displacements of the dam are similar to one another. All the three kinds of boundaries are suitable when we focus on the vertical response only. The difference between the maximums of relative displacements in X direction obtained by using three boundaries decreased with the increase in the dam height. In particular, the difference of maximum relative displacements in the horizontal direction obtained by using three boundaries is large at a low height position of the dam. The dynamic analysis accuracies of the three boundaries are similar to one another, according to the analysis conclusion of the semi-infinite body above. In Figure 24, the difference is mainly caused by the static effect. The static-dynamic comprehensive relative displacement of upstream surface center at a six-meter height position in X direction is depicted in Figure 24. The waveforms of relative displacements obtained by different boundaries are similar to one another. Only the mean level had a fixed difference caused by the static effect. The accuracy of horizontal direction relative displacements obtained by using the boundaries in Methods 1 and 2 are negatively affected when the static load includes horizontal forces. The proposed infinite element boundary method (Method 3) improved the accuracy. For the hydrostructures, which frequently bear the horizontal load, the accuracy of the static-dynamic comprehensive displacement in the horizontal direction is essential. The proposed infinite element boundary method is suitable for the static-dynamic comprehensive problems of hydrostructures.

In addition, we decreased the finite domain foundation simulation range in Method 3 to 1/8 of the original size. We call it Method 4 to distinguish it from Method 3. Figures 22 and 23 show that the decrease in the foundation simulation range did not significantly influence the accuracy of the static-dynamic comprehensive displacement response in X or Z direction at different heights of the dam. Among Methods 1, 2, and 4, Method 4 remains the most accurate. Method 4 improved its computational efficiency while maintaining favorable accuracy in the static-dynamic comprehensive analysis of the gravity dam.

Table 7 presented the analysis times of different boundaries under the same calculation conditions. The infinite element static-dynamic unified boundary had higher computational efficiency.

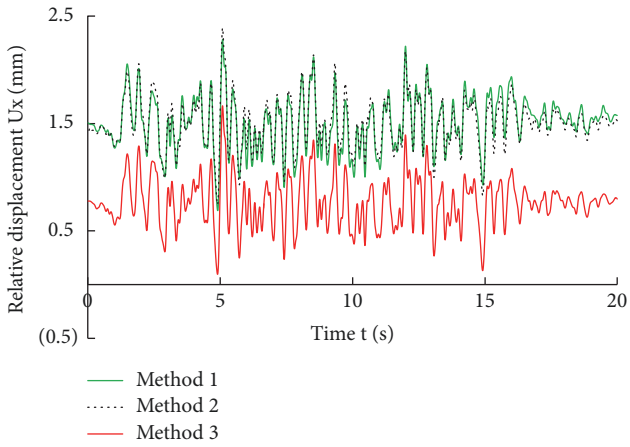

Figure 24: Time history of the X component relative displacement at 6.0 m height of dam.

It is worth mentioning that the discussion of performance, accuracy, and efficiency of different boundaries in this study is under the assumption that the structure is linear elastic. However, for a few hydraulic structures, the nonlinearity of the structure and foundation could not be ignored due to the concrete damage, crack, or the local foundation defect. Infinite element theory and motion equation were deduced and established in frequency domain. The motion equation in time domain could be obtained by Fourier transformation. The solution of any arbitrary point on the boundary depends on the solution of a function or its derivative on the whole boundary. The frequency-time domain transformation leads to a great amount of calculation. Whether the infinite element boundary kept its superiority still or not was paid much attention when it was used in a large-scale nonlinear analysis.

4. Conclusions

To avoid the tedious work of static-dynamic boundary conversion, this paper proposed a new static-dynamic unified artificial boundary based on an infinite element in ABAQUS to solve the static-dynamic synthesis effect conveniently and accurately. The static and dynamic mapping theories of the infinite elements were introduced. The infinite element with zero displacement at infinite faraway was discussed in theory. The equivalent nodal force calculation formula of infinite element unified boundary was deduced from the external wave inputting. The calculation and application program of the equivalent nodal forces was developed using the Python language to complete the external wave inputting. This new method does not require a static and dynamic boundary transformation and import of stress field and constraint counterforce of boundary nodes.

The numerical simulation of a semi-infinite body static, dynamic, and static-dynamic comprehensive calculations was conducted. The results show that a new method is relatively simple and accurate. The calculation precision of the infinite element unified boundary is improved compared with the viscoelastic static-dynamic unified boundary, especially when the static load is in the tangential direction.

Table 7: Analysis times of four different methods.

Methods	t/min
Method 1	136
Method 2	94
Method 3	67
Method 4	43

The numerical simulation of a practical gravity verified the applicability of the infinite element static-dynamic unified boundary for the hydrostructure static-dynamic analysis.

In addition, the foundation simulation range of finite domain can be significantly reduced given the use of infinite element static-dynamic unified boundary. The accuracies of static calculation, dynamic calculation, and static-dynamic comprehensive analysis are unaffected. The proposed infinite element static-dynamic unified boundary improved computational efficiency while maintaining favorable accuracy in the static-dynamic comprehensive analysis of the gravity dam.

Data Availability

The data used to support the findings of this study are available from the corresponding author upon request.

Conflicts of Interest

The authors declare that there are no conflicts of interest regarding the publication of this paper.

Acknowledgments

This research was supported by the National Natural Science Foundation of China (51479165), State Key Laboratory of Eco-hydraulics in Northwest Arid Region of China Independent Research Project (2016ZZKT-1), and Youth Science and Technology New Star Project of Shaanxi Province (2017KJXX-64).

References

[1] Z. P. Liao, H. L. Wong, B. P. Yang et al., "A transmitting boundary for transient wave analyses," *Science China Mathematics*, vol. 27, no. 10, pp. 1063–1076, 1984.

[2] Z. P. Liao, *Introduction to wave motion theories in engineering*, Science Press, Beijing, China, 2002.

[3] J. Lysmer and R. L. Kuhlemeyer, "Finite dynamic model for infinite media," *Journal of Engineering Mechanics*, vol. 95, ASCE, pp. 759–877, 1969.

[4] A. J. Deeks and F. M. Randolph, "Axisymmetric time-domain transmitting boundaries," *Journal of Engineering Mechanics*, vol. 120, ASCE, no. 1, pp. 25–42, 1994.

[5] J. B. Liu and Y. D. Lu, "A direct method for analysis of dynamic soil-structure interaction based on interface idea," in *Dynamic Soil-Structure Interaction*, C. H. Zhang and J. P. Wolf, Eds., pp. 258–273, International Academia Publishers, Beijing, China, 1997.

[6] J. B. Liu, Z. Y. Wang, X. L. Du, and Y. X. Du, "Three-dimensional visco-elastic artificial boundaries in time domain for wave motion problems," *Journal of Engineering Mechanics*, vol. 22, no. 6, pp. 46–51, 2005.

[7] W. J. Lei and D. M. Wei, "Spring-viscous boundary in finite element analyses for infinite media," *Earthquake Engineering and Engineering Vibration*, vol. 25, no. 3, pp. 110–114, 2005.

[8] Y.-H. Liu, B.-Y. Zhang, and H.-Q. Chen, "Comparison of spring-viscous boundary with viscous boundary for arch dam seismic input model," *Journal of Hydraulic Engineering*, vol. 37, no. 6, pp. 758–763, 2006.

[9] J. T. He, H. F. Ma, B. Y. Zhang et al., "Method and realization of seismic motion input of viscous-spring boundary," *Journal of Hydraulic Engineering*, vol. 41, no. 8, pp. 960–969, 2010.

[10] R. F. Ungless, *An Infinite Finite element*, UK: University of British Columbia, 1973.

[11] P. Bettess and O. C. Zienkiewicz, "Diffraction and refraction of surface waves using finite and infinite elements," *International Journal for Numerical Methods in Engineering*, vol. 13, pp. 1271–1290, 1977.

[12] P. Bettess, "More on infinite elements," *International Journal for Numerical Methods in Engineering*, vol. 16, pp. 1613–1626, 1980.

[13] P. Bettess, C. Emson, and T. C. Chiam, *A New Mapped Infinite Element for Exterior Wave Problems*, pp. 489-504, John Wiley & Sons, New York, NY, USA, 1984.

[14] O. C. Zienkiewicz, K. Bando, P. Bettess, C. Emson, and T. C. Chiam, "Mapped infinite elements for exterior wave problems," *International Journal for Numerical Methods in Engineering*, vol. 21, no. 7, pp. 1229–1251, 1985.

[15] P. Bettess, *Infinite Element*, UK: Penshaw Press, 1992.

[16] C. B. Zhao, "Coupled method of finite and dynamic infinite elements for simulating wave propagation in elastic solids involving infinite domains," *Science China: Technological Sciences*, vol. 53, no. 6, pp. 1678–1687, 2010.

[17] C. B. Zhao, C. H. Zhang, and G. D. Zhang, "Simulation of semi-infinite plane elastic foundation using infinite elements," *Journal of Tsinghua University*, vol. 26, no. 3, pp. 51–64, 1986.

[18] C. B. Zhao, *Research on the Infinite Domain Simulation and Seismic Wave Input of Arch Dam Foundation*, pp. 14-42, Tsinghua University, Beijing, China, 1987.

[19] L. B. Yan, *Interaction analysis method and application on the structure and rock and soil medium*, pp. 2-62, Guangxi University, Guangxi, China, 2004.

[20] Y. Jiang, G. H. Chen, and Y. H. Yao, "Application of finite element and infinite element method to stress analysis of gravity dam," *Engineering Journal of Wuhan University*, vol. 42, no. 3, pp. 322–325, 2009.

[21] C. B. Yun and J. m. Kim, *Dynamic Infinite Elements for Soil-Structure Interaction Analysis in a Layered Soil Medium*, vol. 7, no. 4, Springer, Berlin, Germany, 2006.

[22] Doo-Kie, C. B. Yun, and Chung-Bang, "Time-domain soil-structure interaction analysis in two-dimensional medium based on analytical frequency-dependent infinite elements," *International Journal for Numerical Methods in Engineering*, vol. 47, no. 7, pp. 1241–1261, 2015.

[23] Y. L. Qi and K. Otsuka, "Research on artificial boundary of ABAQUS dynamic infinite element," *Rock and Soil Mechanics*, vol. 35, no. 10, pp. 3007–3013, 2014.

[24] F. Gao and F. B. Zhao, "Study on transformation method for artificial boundaries in static-dynamic analysis of underground structure," *Journal of Vibration and Shock*, vol. 30, no. 11, pp. 165–170, 2011.

[25] J. B. Liu and B. Li, "3D visco-elastic static-dynamic uniform artificial boundary," *Science in Chinese: Series E*, vol. 35, no. 9, pp. 966–980, 2005.

[26] C. B. Zhao, C. H. Zhang, and G. D. Zhang, "Studies on the characteristics of dynamic mapping infinite elements," *Earthquake Engineering and Engineering Vibration*, vol. 7, no. 3, pp. 1–15, 1987.

[27] H.-Q. Chen, "Discussion on seismic input mechanism at dam site," *Journal of Hydraulic Engineering*, vol. 37, no. 12, pp. 1417–1423, 2006.

[28] C. J. Cheng and Y. Y. Zhu, *Elasticity mechanics*, Shanghai University Press, Shanghai, China, 2005.

[29] Z. L. Xu, *Elasticity mechanics*, Higher Education Press, Beijing, China, 1990.

[30] National Energy Administration of China, "Code for seismic design of hydraulic structures of hydropower project," NB 35047-2015, 2015.

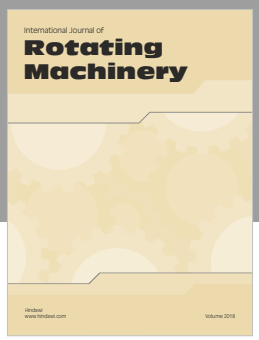

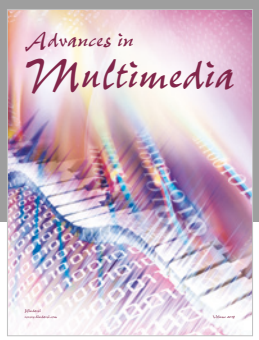

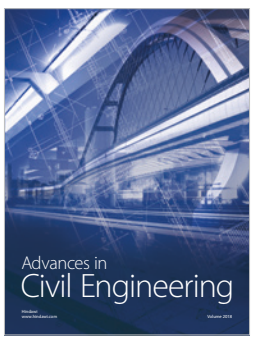

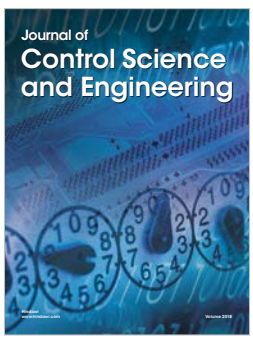

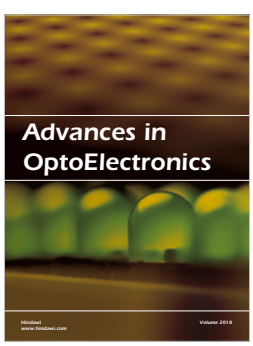

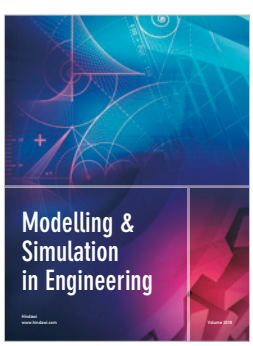

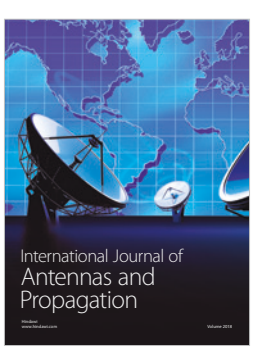

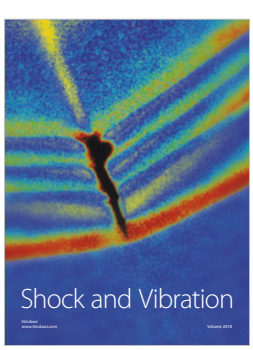

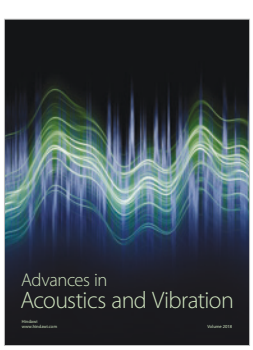

Hindawi

Submit your manuscripts at
www.hindawi.com